Spatial and Orientation Control of Cylindrical Nanostructures in ABA Triblock Copolymer Thin Films by Raster Solvent Vapor Annealing

Jonathan E. Seppala, Ronald L. Lewis, III, and Thomas H. Epps, III*

Department of Chemical & Biomolecular Engineering, University of Delaware, Newark, Delaware 19716, United States

ABSTRACT We present a spatially resolved approach for the solvent vapor annealing (SVA) of block copolymer thin films that permits the facile and relatively rapid manipulation of nanoscale ordering and nanostructure orientation. In our method, a localized (point) SVA zone is created through the use of a vapor delivery nozzle. This point annealing zone can be rastered across the thin film using a motorized stage to control the local nanoscale structure and orientation in a cylinder-forming ABA triblock copolymer thin film. At moderate rastering speeds (~100 μm/s) (*i.e.*, relatively modest annealing time at a given point), the film displayed ordered cylindrical nanostructures with the cylinders oriented parallel to the substrate surface. As the rastering speed was decreased (~10 μm/s), the morphology transformed into a surface nanostructure indicative of cylinders oriented perpendicular to the substrate surface. These perpendicular cylinder orientations also were created by rastering multiple times over the same region, and this effect was found when rastering in either retrace (overlapping) or crossed-path (orthogonal) geometries. Similar trends in nanostructure orientation and ordering were obtained from various nozzle diameters by accounting for differences in solvent flux and annealing time, illustrating the universality of this approach. Finally, we note that our "stylus-based" raster solvent vapor annealing technique allows a given point to be solvent annealed approximately 2 orders of magnitude faster than conventional "bell jar" solvent vapor annealing.

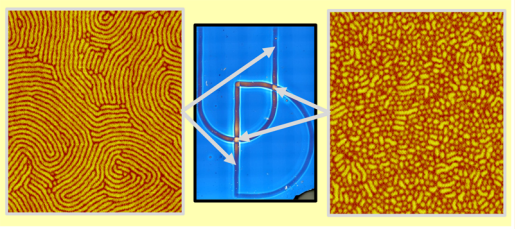

KEYWORDS: solvent vapor annealing · morphology · block copolymer · thin film · nanostructure · annealing · raster · zone annealing

The commercial feasibility of many emerging nanotechnologies requires precise control of nanoscale structures over large areas. Self-assembly processes in block copolymer (BCP) thin films provide the opportunity to create designer nanoscale materials for nanoporous membranes,[1−3] lithographic masks,[1,4,5] and nanopatterning/templating applications,[6−11] of which the latter two applications have been investigated for the production of organic and optoelectronics[12−14] and high-density storage devices.[15] Additionally, block copolymer thin films offer ideal structures for heterojunction organic photovoltaics (~10 nm wide interdigitated domains) due to their ability to form co-continuous or perpendicularly oriented phases with domain spacings on similar size scales to exciton diffusion lengths.[12,14,16,17]

Many of the above nanotechnologies take advantage of morphologies common to AB diblock and ABA triblock copolymers (spheres, cylinders, gyroid, and lamellae), where the thermodynamics of bulk self-assembly is relatively well understood.[18,19] Briefly, three major variables influence the morphology of bulk block copolymers: the degree of polymerization (N), the interaction parameter (χ) where χN is the segregation strength, and the volume fraction of the blocks (f).[19−21] For thin films, where the surfaces strongly effect the final nanoscale morphology, commensurability between the film thickness and the copolymer domain spacing along with polymer−surface interactions (surface energy or surface chemistry) can influence both the morphology's symmetry and orientation.[22] In many cases, thermal annealing or solvent annealing is used to facilitate copolymer self-assembly by imparting mobility to glassy and/or entangled regions that are often kinetically trapped upon casting. In addition to imparting increased chain motion, many annealing protocols also are employed to manipulate the nanostructure orientation in BCP thin films.

Thermal annealing can promote perpendicular (or parallel) cylinders[23,24] or lamellae[23] by creating a neutral (or preferential) free surface; however, the effect often is limited to systems containing blocks with

* Address correspondence to thepps@udel.edu.

Received for review July 30, 2012 and accepted October 1, 2012.

Published online October 04, 2012
10.1021/nn303416p

similar surface energies for perpendicular orientations and systems that do not contain thermally sensitive or thermally responsive polymers, such as *t*-butyl acrylate.[24−29] An alternative approach, solvent vapor annealing (SVA), provides mobility by effectively decreasing the T_g of the copolymers[30,31] and can direct nanoscale self-assembly in several ways. For example, solvent in the film alters block−block interactions (χ_{eff}) and enhances (or mitigates) free and substrate surface interactions.[30,32−35] Solvent swelling also changes both the domain spacing and overall film thicknesses, effecting commensurability and thus influencing the orientation of the copolymer nanostructure.[33,36−38] Furthermore, selective swelling of one block can alter the thin film morphology by shifting the relative component volume fractions,[39−42] while solvent affinity for the minority block(s) can play an additional role in the orientation of some morphologies *via* preferred diffusion routes.[43] Finally, controlled deswelling can direct nanostructure orientation in response to moderated changes in film thicknesses.[44,45]

Control over morphology and orientation in small batch processes, typical of thermal and solvent annealing experiments, is not sufficient for the large-scale production of BCP thin film nanotechnologies. Continuous methods such as roll-to-roll or web-based fabrication are required to achieve low-cost production of BCP-based products.[46] In the literature, there are several examples of zone-based methods adapted from small molecule crystals[47] or metallurgy and semiconductor processing[48,49] that are amenable to continuous processing of BCP thin films. For example, Tang and co-workers demonstrated ordering of parallel and perpendicular oriented lamellae[47,50] and perpendicular oriented cylinders[50] by zone casting directly from solution, where a controlled flow of polymer solution was placed onto a moving substrate creating an evaporation/solidification front. A combination of solution flow rate, substrate speed, and solvent evaporation rate (by manipulating temperature) was used to manipulate the advancing evaporation/solidification front, generating nanoscale order over tens of micrometers in a continuous process. However, parallel alignment of lamellae was only achieved by changing to a crystallizable block, creating a crystallization front normal to the solidification front. Hashimoto and co-workers also described alignment and preferential orientation of lamellae and cylinder-forming BCP thick (bulk) films using a "zone heating device".[51] In zone heating, the film is passed over a narrow heating zone surrounded by a pair of cooling zones, creating a thermal front above (hot zone annealing)[51−55] or below (cold zone annealing)[56] the order−disorder transition (ODT) temperature (T_{ODT}).[49,56] One example of BCP thin film hot zone annealing (HZA) by Angelescu used a resistive heater and function generator to create a sweeping (oscillatory) thermal gradient.[48] Although

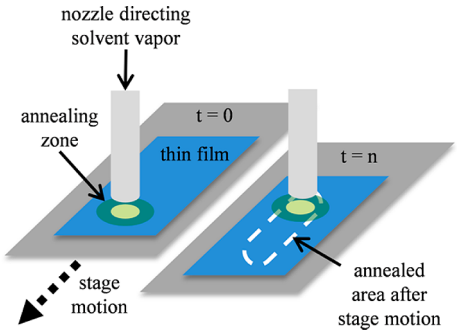

Figure 1. Illustration of RSVA apparatus. Solvent vapor from a bubbler system was directed onto the surface of a block copolymer thin film creating a SVA zone (left side). Rastering the SVA zone by moving the film with a motorized stage created a localized annealed area (right side).

not directly amenable to continuous processing, the oscillating solidification front produced highly ordered cylinders covering square millimeters. Jones and co-workers applied cold zone annealing (CZA) to a cylinder-forming BCP thin film.[49,57] Unlike HZA, where ordering occurs as a solidification or phase separation front when the BCP falls below T_{ODT} upon exiting the heating zone, BCPs annealed by CZA are in the strong segregation regime ($T \ll T_{ODT}$) with an ordering front at the approach of the heating zone. Jones and co-workers' experiments showed enhanced ordering kinetics, preferential alignment, and defect-free long-range order in parallel oriented cylinders. Unfortunately, HZA and CZA are thermal annealing methods and thus share the limitations found in classical (static) thermal annealing, where ordering is directed primarily by block−block and block−surface interactions. Adapting SVA as a zone method incorporates the advantages of thermal zone annealing (continuous processing and enhanced ordering kinetics) and SVA (compatibility with thermally responsive polymers and a large parameter space for morphology and orientation control).

To the author's knowledge, the zone annealing of BCPs using solvent vapor remains unexplored, and examples of solvent zone annealing in the literature are primarily limited to organic semiconductors.[58,59] Thus, we report the design and characterization of a SVA analogue to thermal zone annealing for BCPs with the added benefit of spatial control over morphology, here termed raster solvent vapor annealing (RSVA). By combining SVA and zone processing, RSVA offers some unique advantages over classic "bell jar" or flow chamber annealing methods. In typical SVA experiments, solvent vapor equilibrium is maintained by the solvent vapor pressure in a sealed system or solvent uptake by a carrier gas, usually N_2, into a flow chamber setup.[22] In either case, transport of solvent vapor to the film surface is diffusive, by nature of the setup, and an equilibrium−swelling ratio (or film dewetting)[22] is reached after a sufficient time (minutes to hours).[38,60] Thus, a uniform surface field directs the self-assembly

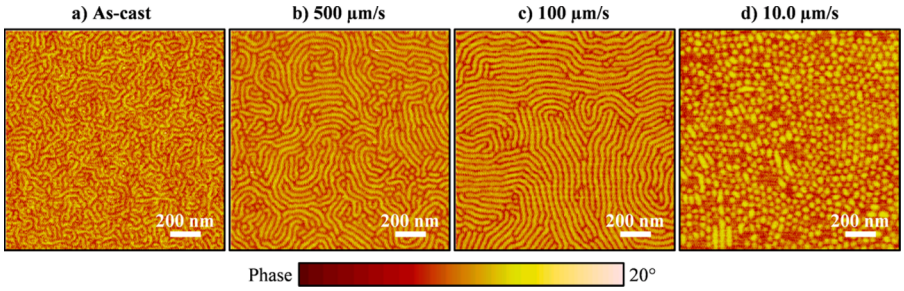

Figure 2. AFM phase images of a single-pass RSVA with a 0.514 mm i.d. nozzle and 30 mL/min THF bubbler N_2 flow rate at decreasing RSVA speeds, taken at the center of the annealed area. (a) As-cast example of phase-separated nanostructure with minimal long-range order; (b) 500 μm/s, parallel oriented cylinders; (c) 100 μm/s, parallel oriented cylinders with greater long-range order; (d) 10 μm/s, primarily perpendicular oriented cylinders. RSVA direction was from left to right in all images.

across the entire film. RSVA, which uses a nozzle to direct the solvent vapor, provides convective transport (nearly instantaneous film swelling), spatial fidelity of annealing, and, when coupled with a motorized stage, finite control over the annealed areas (see Figure 1). This geometry provides the same basic effect of HZA or CZA with the additional benefits of the improved flexibility afforded by solvent vapor annealing (such as tunable mitigation of block−block interactions, block volume fractions, and surface fields).

RESULTS AND DISCUSSION

Raster solvent vapor annealing was accomplished using a tetrahydrofuran (THF)-rich vapor stream in single or multiple pass(es) over a 100 nm thick (~3.5L_0) poly(styrene-*b*-isoprene-*b*-styrene) (SIS) film (domain spacing of ~29 nm). RSVA speeds (speed of the motorized stage relative to the fixed nozzle) spanning 500 μm/s to 3 μm/s were employed to generate spatially resolved regions with nanoscale cylinders oriented either parallel or perpendicular to the substrate surface. Solvent uptake or swelling was nearly instantaneous (to the naked eye) and thus independent of the RSVA speed over the studied range. As the annealing zone passed over the film, the film color changed from deep-blue ("as-cast") to green just outside the nozzle radius to tan directly under the nozzle. Though our setup did not permit *in situ* film thickness measurements with the nozzle normal to the surface, a qualitative comparison with the nozzle angled to 45° (where solvent swollen film thickness measurements could be obtained *in situ* using a spectral reflectometer)[45] was employed to estimate the film thickness. Thus, we determined that the SIS film under RSVA equilibrated to a swollen film thickness of at least 160 nm (~5.5L_0), changing in color from deep-blue (unswollen) to green and tan (swollen) when under direct exposure to the directed solvent vapor stream. Thickness measurements made following completion of the RSVA experiments indicated that the film had dried to near its pre-RSVA thickness of 100 nm, though some samples appeared to contain a minor amount of residual solvent as detailed below. We note that the reported final thickness is an average of rastered and non-rastered regions as the spot size of the spectral reflectometer is ~4× larger than the area directly annealed.

Single-Pass RSVA Nanostructures and Orientations. The "as-cast" nanostructure of our flow-coated SIS films was parallel oriented cylinders with minimal long-range order, as shown in Figure 2a. RSVA with a 0.514 mm i.d. nozzle and THF bubbler N_2 flow rate of 30 mL/min facilitated the ordering of cylinders oriented parallel to the substrate at RSVA speeds above 100 μm/s (see Figure 2b,c). The grain size of the parallel cylinders increased as RSVA speed was reduced (or as annealing time per unit area increased), as shown in Figure 2. RSVA at 100 μm/s was equivalent to an annealing time of ~5 s (nozzle diameter of 0.514 mm moving across the film at 100 μm/s), and the orientation and degree of order in the parallel cylinders was quantitatively equivalent to that of a static 30 min THF bell jar anneal (see Supporting Information Figure S1 for bell jar annealed AFM images).

As the RSVA speed was further reduced, a transformation of the nanostructure orientation was noted. RSVA at a speed of 10 μm/s (an annealing time of ~50 s per nozzle diameter) led to a surface nanostructure indicative of cylinders oriented perpendicular to the substrate surface (see Figure 2d).[38] In comparison, THF bell jar and flow chamber SVA of SIS films of similar thickness typically result in parallel orientations and, after sufficient time, dewetting.[38] The perpendicular cylinders from RSVA appeared slightly swollen (postdrying), which was confirmed by comparison of the first peak (q^*) position in the azimuthally integrated 1D profiles from fast Fourier transforms (FFTs) of the AFM images (see Supporting Information Figure S2 for 1D profiles). Instead of the expected $2/(\sqrt{3})$ ratio of $q^*_{perpendicular}$ to $q^*_{parallel}$, we find a ratio closer to 0.84. This discrepancy could result from a combination of the lack of hexagonal order as well as residual solvent that leaves the PS cylinders slightly swollen. However, Konrad *et al.* provides an alternative explanation in their radio frequency etching study of cylinder-forming poly(styrene-*b*-butadiene-*b*-styrene)

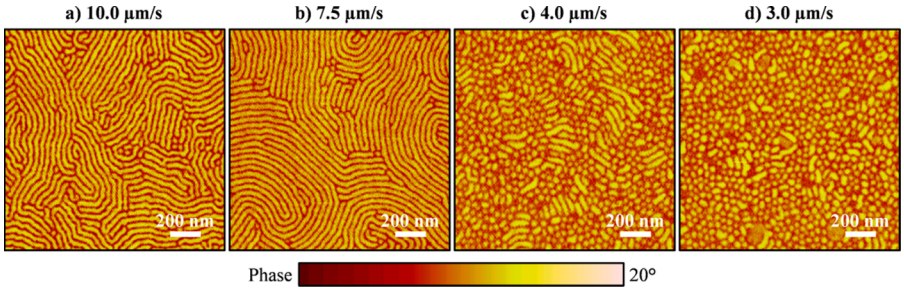

Figure 3. AFM phase images of a single-pass RSVA with a 0.210 mm i.d. nozzle and 5 mL/min THF bubbler N_2 flow rate at decreasing RSVA speeds: (a) 10 μm/s, parallel oriented cylinders; (b) 7.5 μm/s, parallel oriented cylinders exhibiting greater long-range order; (c) 4 μm/s, primarily perpendicular oriented cylinders with a significant fraction of short parallel cylindrical nanostructures; (d) 3 μm/s, primarily perpendicular oriented cylinders.

thin films.[61] They describe perpendicular cylinders protruding as "necks" from an underlying parallel cylinder nanostructure where the ratio of the cylinder-to-cylinder spacing of perpendicular necks to parallel cylinders is $2/(\sqrt{3})$ or 1.155. Experimentally, they measured ratios of 1.09 to 1.22. The ratio of our cylinder-to-cylinder spacing for perpendicular to parallel cylinders is 1.19, based on image analysis of AFM micrographs. Additionally, we note that the perpendicular structures appear to result from the breakup of parallel cylinders as the transition between the two cylinder orientations can be noted in Figure 3c,d.

When the nozzle was changed to a smaller diameter (0.210 mm i.d.), the THF bubbler N_2 flow rate was decreased to 5 mL/min, keeping the solvent vapor flux constant. RSVA at 10 and 7.5 μm/s with the 0.210 mm i.d. nozzle promoted parallel orientations of cylinders, where the lower of the two speeds resulted in increased ordering (see Figure 3a,b). A further reduction in the RSVA speeds to 4 and 3 μm/s produced morphologies indicative of primarily perpendicular orientations of cylinders (with the remainder oriented parallel to the substrate), as shown in Figure 3c,d. We note that the fraction of perpendicular cylinders increased at the lower of the two speeds. Although the smaller nozzle (0.210 mm i.d.) required slower RSVA speeds in order to achieve similar degrees of cylinder order and orientation when compared to the larger nozzle (0.514 mm i.d.), the results are consistent with a reduction in total annealing time per unit distance given the smaller annealing area at equivalent RSVA speeds. Nearly equivalent annealing times occurred at RSVA speeds of 4 μm/s with the 0.210 mm i.d. nozzle (THF bubbler N_2 flow rate of 5 mL/min) and 10 μm/s with the 0.514 mm i.d. nozzle (THF bubbler N_2 flow rate of 30 mL/min), 52.5 and 51.4 s, respectively. The predominant features indicated cylinders oriented perpendicular to the substrate under both nozzle configurations, as illustrated by Figures 2d and 3c.

The final nanostructure resulting from RSVA at different speeds was a balance between several competing forces. Polyisoprene (PI), the majority block, had a lower surface energy than polystyrene (PS), 32.0 mJ/m^2 *versus* 40.7 mJ/m^2,[62] and preferred to "wet" both the free and substrate surface leading to a parallel orientation of the cylinder morphology.[63] At high RSVA speeds, the preferential surface interactions were maintained, and the nanostructure retained its parallel orientation. These surface energy differences between the PS and PI likely were strong enough to overcome the entropic penalties (looping of the middle block at the film's top and bottom surfaces) incurred by the PI block[64] and (loss of free chain ends at the surface) incurred by the PS block[65] in the parallel configuration. At sufficiently low RSVA speeds (*i.e.*, longer annealing times for a given point), the solvent vapor annealing likely contributed to the formation of cylinders oriented perpendicular to the substrate surface in several ways. First, the solvent lowered the surface energy difference between the blocks, allowing either the entropic bending penalty of the middle PI block[64] or the entropic drive for locating free chain ends near the surface[65] to dominate. Second, the initial swelling and subsequent deswelling of the thin film cycled the BCP film through a series of commensurate and incommensurate thickness conditions, which perpendicular orientations of cylinders can better accommodate by avoiding the entropic stretching penalty associated with parallel orientations of cylinders.[33,45,63,66,67] Finally, the perpendicular orientations of cylinders appeared to form following the breakup of parallel cylinders,[68] again supporting the formation of parallel cylinders at shorter annealing times (or faster RSVA speeds) and perpendicular cylinders at longer annealing times (or slower RSVA speeds), as shown in Figure 3c,d. We also note that the slower RSVA speeds likely lead to slower deswell rates, which is also known to induce perpendicular cylinder orientations that propagate from the free surface down toward the substrate in SIS thin films;[45] this effect will be investigated in future studies.

Multiple-Pass RSVA Nanostructures and Orientations. RSVA speed was not the only method for controlling cylinder ordering and orientations, as multiple RSVA passes over the same area showed a similar effect. Multipass RSVA with the 0.514 mm i.d. nozzle (THF bubbler N_2

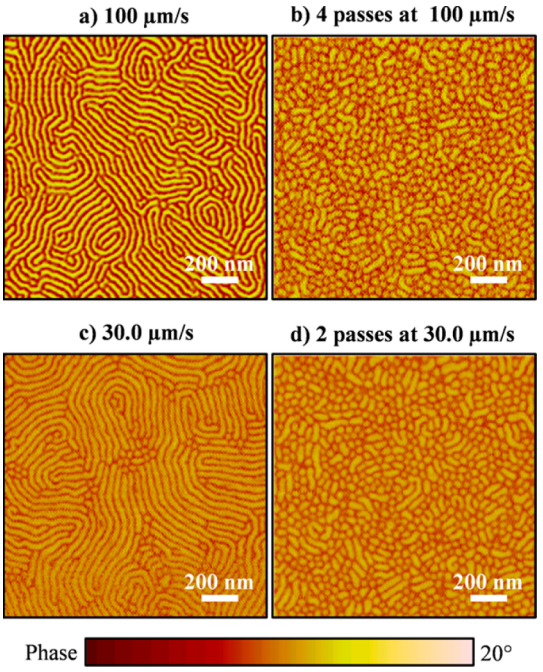

Figure 4. AFM phase images of single- and multiple-pass RSVA with 0.514 mm i.d. nozzle and 30 mL/min THF bubbler N_2 flow rate. (a) Single pass at 100 μm/s, parallel oriented cylinders; (b) four passes at 100 μm/s, primarily perpendicular oriented; (c) single pass at 30 μm/s, parallel oriented cylinders; (d) two passes at 30 μm/s, primarily perpendicular oriented cylinders.

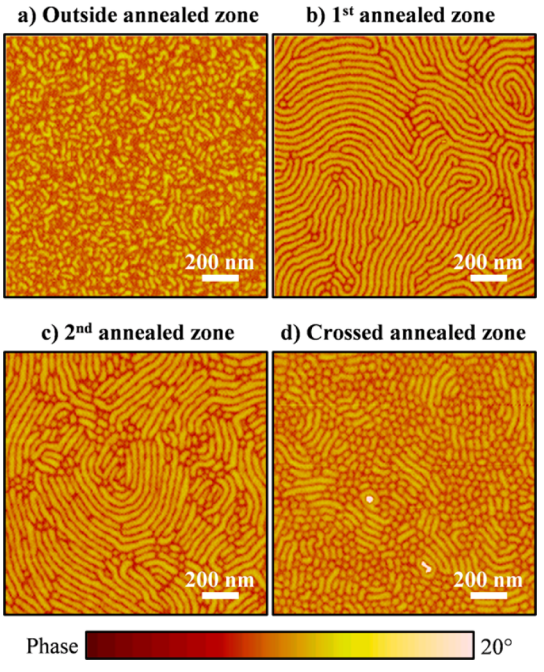

Figure 5. AFM phase images of crossed-path RSVA with 0.514 mm i.d. nozzle, 30 mL/min THF bubbler N_2 flow rate, and fixed RSVA speed of 30 μm/s. (a) Area outside RSVA zone; (b) area in first RSVA zone, single pass; (c) area in second (orthogonal) RSVA zone, single pass; (d) area where RSVA zones in panels b and c crossed paths, *i.e.*, two passes.

flow rate of 30 mL/min) at speeds of 100 and 30 μm/s resulted in perpendicular orientations of cylinders following four passes (100 μm/s) or two passes (30 μm/s), as displayed in Figure 4. For the 100 μm/s RSVA samples, a single pass resulted in parallel cylinders (Figure 4a), while a series of four passes led to the formation of perpendicular cylinders (Figure 4b). A similar effect was noted for the 30 μm/s RSVA samples, where a single pass resulted in parallel cylinders (Figure 4c), while a second pass led to the formation of perpendicular cylinders (Figure 4d). In this case, only two passes were needed at the lower RSVA speed due to the concomitant increase in annealing time per unit area. The annealing times appear additive with a minimum annealing time of ~20 s required to produce perpendicular nanostructures, achieved in 4 passes at 100 μm/s and in 1.2 passes at 30 μm/s. This minimum annealing time is supported by the single-pass results in Figures 2 and 3.

Crossed-Path RSVA Nanostructures and Orientations. Given the ability of multiple passes to alter the nanoscale orientation of the cylindrical domains, "crossed-path" RSVA provided the opportunity to generate spatially defined parallel and perpendicular orientations of cylinders on a single substrate. More specifically, the above results show that the surface orientation of the cylindrical domains can be switched from parallel to perpendicular in a specific location by making a second RSVA pass over an annealed area. An example of crossed-path RSVA using two orthogonal passes is presented in Figure 5. In this experiment, the film was RSVAed at 30 μm/s using the 0.514 mm i.d. nozzle (THF bubbler N_2 flow rate of 30 mL/min), then rotated 90° and RSVAed a second time under the same conditions. This treatment procedure created a "cross-shaped" annealed area with regions of as-cast, single-pass RSVAed film and double-pass RSVAed film. Areas annealed by only a single RSVA at 30 μm/s exhibited parallel orientations of cylinders (see Figure 5b,c), similar to the example in Figure 4. At the center of the crossed-path RSVA area, perpendicular orientations of cylinders dominated the thin film (see Figure 5d), as expected based on Figure 4 (intermediate regions, between Figure 5b,d, are available in the Supporting Information Figure S3). In regions outside either the first or second RSVA passes, the nanostructure was nanoscale cylinders with minimal ordering, similar to an as-cast condition (see Figures 5a and 2a).

CONCLUSIONS

Raster solvent vapor annealing (RSVA) provided a spatially controlled method for promoting order and reorientation of nanoscale domains in cylinder-forming ABA triblock copolymer thin films. Spatial control of nanostructure orientation was achieved through a motorized $x-y$ stage and mass flow controllers to manipulate the solvent vapor feed. Moderate RSVA speeds (~5 s per nozzle diameter) promoted the formation of cylinders oriented parallel to the substrate

surface, with the nanostructure's grain size increasing as RSVA speed was moderately decreased (*e.g.*, annealing time increased). Slow RSVA speeds (~50 s per nozzle diameter) promoted the formation of dot patterns indicative of cylinders oriented perpendicular to the substrate surface. The perpendicular cylinders appeared to form following a gradual breakup of the parallel cylinders as annealing time grew (either *via* slower RSVA speed in a single pass or through an increased number of passes). We note that our RSVA allows a given point to be solvent annealed approximately 2 orders of magnitude faster than conventional bell jar solvent vapor annealing. Finally, this "stylus-based" annealing method can be adapted to other nozzle shapes such as slit geometries, and additional parameters such as solvent quality and substrate temperature can be manipulated to alter the annealing profile.

METHODS

Thin Film Preparation. Poly(styrene-*b*-isoprene-*b*-styrene) (SIS) (Vector V4211a, DEXCO Polymer, Inc.) was flow coated[69] from a 2 wt % solution in tetrahydrofuran (THF) (Optima HPLC grade, Fisher Scientific, purified though 2 neutral alumina columns) onto polished silicon substrates (Wafer World, N<100>). The block copolymer had a number average molecular weight of 118 kg/mol, polydispersity index of 1.09, and block volume fractions of $f_{PS} = 0.134$, $f_{PI} = 0.732$, and $f_{PS} = 0.134$ (determined from the homopolymer densities at 140 °C).[70] Small-angle X-ray scattering (SAXS) indicated a bulk cylinder morphology with a domain spacing (L_0) of 29 nm (calculated from the primary SAXS peak). Silicon substrates were triple rinsed with toluene (ACS grade, Fisher Scientific, purified through a neutral alumina and a Q5 catalyst column), UVO-cleaned (model 342, Jelight Co., Inc.), and then rerinsed with toluene. Flow coating was accomplished by injecting 75 μL of the polymer solution under a 1 in. wide glass blade held 200 μm above a wafer affixed to a programmable motorized stage.[69] Uniform films (100 $\pm$ 2 nm in thickness and 60 mm in length) were produced using a velocity of 15 mm/s with an acceleration of 0.1 mm/s^2. Film thickness was measured using a FM-20UV spectral reflectometer (Filmetrics, Inc.) with a mass-averaged refractive index.

Thin Film Annealing. Raster solvent vapor annealing was performed using a setup in which N_2 gas was bubbled through THF to produce a solvent-rich vapor stream. The vapor stream was directed onto the film using a nozzle. The nozzles were constructed from 21 or 27 gauge hypodermic needles, 0.514 or 0.210 mm i.d., respectively. The needles were ground flat and attached to a vertical micrometer stage set 0.5 mm above the film surface for the 0.514 mm i.d. nozzle and 0.1 mm for the 0.210 mm i.d. nozzle. The substrate-supported films were affixed to a programmable motorized stage to control the rastering speed and position. RSVA experiments were conducted under ambient conditions (~22 °C, <20% relative humidity). RSVA experiments with multiple passes were dried under vacuum at 50 °C for 30 min between each pass.

AFM Characterization. Atomic force microscopy (AFM) phase images were obtained on a Bruker Veeco Dimension 3100 with Nanoscope V controller operating in tapping mode using Budget Sensors TAP150-G tips (150kHz, 5 N/m). Images were taken in the center of the annealed area along the rastering direction unless otherwise noted. Phase images in the text are displayed with the RSVA direction from left to right.

Conflict of Interest: The authors declare no competing financial interest.

Acknowledgment. This work was supported by the National Science Foundation (NSF) through an NSF CAREER grant, DMR-0645586. We acknowledge a DuPont Young Professor Grant for additional support. We thank the W. M. Keck Electron Microscopy Facility at the University of Delaware for the use of their AFM facilities. We also thank J. Albert, M. Luo, and J. Emerson for helpful discussions.

Supporting Information Available: AFM phase image of SIS film after 30 min THF "bell jar" anneal in Figure S1. One-dimensional profiles of azimuthally integrated FFTs obtained from the AFM phase images in Figure S2. AFM phase images of crossed-path RSVA along first raster direction in Figure S3. This material is available free of charge *via* the Internet at http://pubs.acs.org.

Note Added after ASAP Publication: This paper was inadvertently published on the Web October 4, 2012, before author corrections were applied. The corrected version was reposted October 5, 2012.

REFERENCES AND NOTES

1. Fasolka, M. J.; Mayes, A. M. Block Copolymer Thin Films: Physics and Applications I. *Annu. Rev. Mater. Res.* **2001**, *31*, 323–355.
2. Phillip, W. A.; O'Neill, B.; Rodwogin, M.; Hillmyer, M. A.; Cussler, E. L. Self-Assembled Block Copolymer Thin Films as Water Filtration Membranes. *ACS Appl. Mater. Interfaces* **2010**, *2*, 847–853.
3. Jackson, E. A.; Hillmyer, M. A. Nanoporous Membranes Derived from Block Copolymers: From Drug Delivery to Water Filtration. *ACS Nano* **2010**, *4*, 3548–3553.
4. Chang, S.-W.; Chuang, V. P.; Boles, S. T.; Ross, C. A.; Thompson, C. V. Densely Packed Arrays of Ultra-High-Aspect-Ratio Silicon Nanowires Fabricated Using Block-Copolymer Lithography and Metal-Assisted Etching. *Adv. Funct. Mater.* **2009**, *19*, 2495–2500.
5. Tang, C.; Lennon, E. M.; Fredrickson, G. H.; Kramer, E. J.; Hawker, C. J. Evolution of Block Copolymer Lithography to Highly Ordered Square Arrays. *Science* **2008**, *322*, 429–432.
6. Chao, C.-C.; Wang, T.-C.; Ho, R.-M.; Georgopanos, P.; Avgeropoulos, A.; Thomas, E. L. Robust Block Copolymer Mask for Nanopatterning Polymer Films. *ACS Nano* **2010**, *4*, 2088–2094.
7. Pavan, M. J.; Shenhar, R. Two-Dimensional Nanoparticle Organization Using Block Copolymer Thin Films as Templates. *J. Mater. Chem.* **2011**, *21*, 2028–2040.
8. Park, S.; Kim, B.; Wang, J. Y.; Russell, T. P. Fabrication of Highly Ordered Silicon Oxide Dots and Stripes from Block Copolymer Thin Films. *Adv. Mater.* **2008**, *20*, 681–685.
9. Jung, Y. S.; Ross, C. A. Well-Ordered Thin-Film Nanopore Arrays Formed Using a Block-Copolymer Template. *Small* **2009**, *5*, 1654–1659.
10. Son, J. G.; Bae, W. K.; Kang, H.; Nealey, P. F.; Char, K. Placement Control of Nanomaterial Arrays on the Surface-Reconstructed Block Copolymer Thin Films. *ACS Nano* **2009**, *3*, 3927–3934.
11. Bang, J.; Jeong, U.; Ryu, D. Y.; Russell, T. P.; Hawker, C. J. Block Copolymer Nanolithography: Translation of Molecular Level Control to Nanoscale Patterns. *Adv. Mater.* **2009**, *21*, 4769–4792.
12. Botiz, I.; Darling, S. B. Optoelectronics Using Block Copolymers. *Mater. Today* **2010**, *13*, 42–51.
13. Chen, J.; Frisbie, C. D.; Bates, F. S. Lithium Perchlorate-Doped Poly(styrene-*b*-ethylene oxide-*b*-styrene) Lamellae-Forming Triblock Copolymer as High Capacitance, Smooth, Thin Film Dielectric. *J. Phys. Chem. C* **2009**, *113*, 3903–3908.
14. Segalman, R. A.; McCulloch, B.; Kirmayer, S.; Urban, J. J. Block Copolymers for Organic Optoelectronics. *Macromolecules* **2009**, *42*, 9205–9216.
15. Ruiz, R.; Kang, H.; Detcheverry, F. A.; Dobisz, E.; Kercher, D. S.; Albrecht, T. R.; de Pablo, J. J.; Nealey, P. F. Density

Multiplication and Improved Lithography by Directed Block Copolymer Assembly. *Science* **2008**, *321*, 936–939.
16. Coakley, K. M.; McGehee, M. D. Conjugated Polymer Photovoltaic Cells. *Chem. Mater.* **2004**, *16*, 4533–4542.
17. Darling, S. B. Block Copolymers for Photovoltaics. *Energy Environ. Sci.* **2009**, *2*, 1266–1273.
18. Bates, F. S.; Schulz, M. F.; Khandpur, A. K.; Forster, S.; Rosedale, J. H.; Almdal, K.; Mortensen, K. Fluctuations, Conformational Asymmetry and Block Copolymer Phase Behaviour. *Faraday Discuss.* **1994**, *98*, 7–18.
19. Matsen, M. W.; Thompson, R. B. Equilibrium Behavior of Symmetric ABA Triblock Copolymer Melts. *J. Chem. Phys.* **1999**, *111*, 7139–7146.
20. Matsen, M. W.; Bates, F. S. Unifying Weak- and Strong-Segregation Block Copolymer Theories. *Macromolecules* **1996**, *29*, 1091–1098.
21. Bates, F. S. Polymer–Polymer Phase-Behavior. *Science* **1991**, *251*, 898–905.
22. Albert, J. N. L.; Epps, T. H., III. Self-Assembly of Block Copolymer Thin Films. *Mater. Today* **2010**, *13*, 24–33.
23. Sivaniah, E.; Hayashi, Y.; Iino, M.; Hashimoto, T.; Fukunaga, K. Observation of Perpendicular Orientation in Symmetric Diblock Copolymer Thin Films on Rough Substrates. *Macromolecules* **2003**, *36*, 5894–5896.
24. Kelly, J. Y.; Albert, J. N. L.; Howarter, J. A.; Kang, S.; Stafford, C. M.; Epps, T. H., III; Fasolka, M. J. Investigation of Thermally Responsive Block Copolymer Thin Film Morphologies Using Gradients. *ACS Appl. Mater. Interfaces* **2010**, *2*, 3241–3248.
25. La, Y.-H.; Stoykovich, M. P.; Park, S.-M.; Nealey, P. F. Directed Assembly of Cylinder-Forming Block Copolymers into Patterned Structures To Fabricate Arrays of Spherical Domains and Nanoparticles. *Chem. Mater.* **2007**, *19*, 4538–4544.
26. La, Y.-H.; Edwards, E. W.; Park, S.-M.; Nealey, P. F. Directed Assembly of Cylinder-Forming Block Copolymer Films and Thermochemically Induced Cylinder to Sphere Transition: A Hierarchical Route to Linear Arrays of Nanodots. *Nano Lett.* **2005**, *5*, 1379–1384.
27. Park, J. H.; Sun, Y.; Goldman, Y. E.; Composto, R. J. Amphiphilic Block Copolymer Films: Phase Transition, Stabilization, and Nanoscale Templates. *Macromolecules* **2009**, *42*, 1017–1023.
28. Xu, C.; Fu, X.; Fryd, M.; Xu, S.; Wayland, B. B.; Winey, K. I.; Composto, R. J. Reversible Stimuli-Responsive Nanostructures Assembled from Amphiphilic Block Copolymers. *Nano Lett.* **2006**, *6*, 282–287.
29. Kelly, J. Y.; Albert, J. N. L.; Howarter, J. A.; Stafford, C. M.; Epps, T. H., III; Fasolka, M. J. Manipulating Morphology and Orientation in Thermally Responsive Block Copolymer Thin Films. *J. Polym. Sci., Part B: Polym. Phys.* **2012**, *50*, 263–271.
30. Cavicchi, K. A.; Berthiaume, K. J.; Russell, T. P. Solvent Annealing Thin Films of Poly(isoprene-*b*-lactide). *Polymer* **2005**, *46*, 11635–11639.
31. Di, Z.; Posselt, D.; Smilgies, D.-M.; Papadakis, C. M. Structural Rearrangements in a Lamellar Diblock Copolymer Thin Film during Treatment with Saturated Solvent Vapor. *Macromolecules* **2009**, *43*, 418–427.
32. Xuan, Y.; Peng, J.; Cui, L.; Wang, H.; Li, B.; Han, Y. Morphology Development of Ultrathin Symmetric Diblock Copolymer Film *via* Solvent Vapor Treatment. *Macromolecules* **2004**, *37*, 7301–7307.
33. Knoll, A.; Magerle, R.; Krausch, G. Phase Behavior in Thin Films of Cylinder-Forming ABA Block Copolymers: Experiments. *J. Chem. Phys.* **2004**, *120*, 1105–1116.
34. Knoll, A.; Horvat, A.; Lyakhova, K. S.; Krausch, G.; Sevink, G. J. A.; Zvelindovsky, A. V.; Magerle, R. Phase Behavior in Thin Films of Cylinder-Forming Block Copolymers. *Phys. Rev. Lett.* **2002**, *89*, 035501.
35. Zettl, U.; Knoll, A.; Tsarkova, L. Effect of Confinement on the Mesoscale and Macroscopic Swelling of Thin Block Copolymer Films. *Langmuir* **2010**, *26*, 6610–6617.
36. Knoll, A.; Tsarkova, L.; Krausch, G. Nanoscaling of Microdomain Spacings in Thin Films of Cylinder-Forming Block Copolymers. *Nano Lett.* **2007**, *7*, 843–846.
37. Cavicchi, K. A.; Russell, T. P. Solvent Annealed Thin Films of Asymmetric Polyisoprene–Polylactide Diblock Copolymers. *Macromolecules* **2007**, *40*, 1181–1186.
38. Albert, J. N. L.; Bogart, T. D.; Lewis, R. L., III; Beers, K. L.; Fasolka, M. J.; Hutchison, J. B.; Vogt, B. D.; Epps, T. H., III. Gradient Solvent Vapor Annealing of Block Copolymer Thin Films Using a Microfluidic Mixing Device. *Nano Lett.* **2011**, *11*, 1351–1357.
39. Jung, Y. S.; Ross, C. A. Solvent-Vapor-Induced Tunability of Self-Assembled Block Copolymer Patterns. *Adv. Mater.* **2009**, *21*, 2540–2545.
40. Chen, Y.; Huang, H.; Hu, Z.; He, T. Lateral Nanopatterns in Thin Diblock Copolymer Films Induced by Selective Solvents. *Langmuir* **2004**, *20*, 3805–3808.
41. Bang, J.; Kim, B. J.; Stein, G. E.; Russell, T. P.; Li, X.; Wang, J.; Kramer, E. J.; Hawker, C. J. Effect of Humidity on the Ordering of PEO-Based Copolymer Thin Films. *Macromolecules* **2007**, *40*, 7019–7025.
42. Li, Y.; Huang, H.; He, T.; Gong, Y. The Effect of the Preferential Affinity of the Solvent on the Microstructure of Solution-Cast Block Copolymer Thin Films. *J. Phys. Chem. B* **2010**, *114*, 1264–1270.
43. Kim, G.; Libera, M. Morphological Development in Solvent-Cast Polystyrene-Polybutadiene-Polystyrene (SBS) Triblock Copolymer Thin Films. *Macromolecules* **1998**, *31*, 2569–2577.
44. Kim, G.; Libera, M. Kinetic Constraints on the Development of Surface Microstructure in SBS Thin Films. *Macromolecules* **1998**, *31*, 2670–2672.
45. Albert, J. N. L.; Young, W.-S.; Lewis, R. L., III; Bogart, T. D.; Smith, J. R.; Epps, T. H., III. Systematic Study on the Effect of Solvent Removal Rate on the Morphology of Solvent Vapor Annealed ABA Triblock Copolymer Thin Films. *ACS Nano* **2012**, *6*, 459–466.
46. Forrest, S. R. The Path to Ubiquitous and Low-Cost Organic Electronic Appliances on Plastic. *Nature* **2004**, *428*, 911–918.
47. Tang, C.; Tracz, A.; Kruk, M.; Zhang, R.; Smilgies, D.-M.; Matyjaszewski, K.; Kowalewski, T. Long-Range Ordered Thin Films of Block Copolymers Prepared by Zone-Casting and Their Thermal Conversion into Ordered Nanostructured Carbon. *J. Am. Chem. Soc.* **2005**, *127*, 6918–6919.
48. Angelescu, D. E.; Waller, J. H.; Adamson, D. H.; Register, R. A.; Chaikin, P. M. Enhanced Order of Block Copolymer Cylinders in Single-Layer Films Using a Sweeping Solidification Front. *Adv. Mater.* **2007**, *19*, 2687–2690.
49. Berry, B. C.; Bosse, A. W.; Douglas, J. F.; Jones, R. L.; Karim, A. Orientational Order in Block Copolymer Films Zone Annealed below the Order–Disorder Transition Temperature. *Nano Lett.* **2007**, *7*, 2789–2794.
50. Tang, C.; Wu, W.; Smilgies, D.-M.; Matyjaszewski, K.; Kowalewski, T. Robust Control of Microdomain Orientation in Thin Films of Block Copolymers by Zone Casting. *J. Am. Chem. Soc.* **2011**, *133*, 11802–11809.
51. Hashimoto, T.; Bodycomb, J.; Funaki, Y.; Kimishima, K. The Effect of Temperature Gradient on the Microdomain Orientation of Diblock Copolymers Undergoing an Order–Disorder Transition. *Macromolecules* **1999**, *32*, 952–954.
52. Bodycomb, J.; Funaki, Y.; Kimishima, K.; Hashimoto, T. Single-Grain Lamellar Microdomain from a Diblock Copolymer. *Macromolecules* **1999**, *32*, 2075–2077.
53. Mita, K.; Takenaka, M.; Hasegawa, H.; Hashimoto, T. Cylindrical Domains of Block Copolymers Developed *via* Ordering under Moving Temperature Gradient: Real-Space Analysis. *Macromolecules* **2008**, *41*, 8789–8799.
54. Mita, K.; Tanaka, H.; Saijo, K.; Takenaka, M.; Hashimoto, T. Ordering of Cylindrical Domain of Block Copolymers under Moving Temperature Gradient: Effects of Moving Rate. *Macromolecules* **2008**, *41*, 6780–6786.
55. Mita, K.; Tanaka, H.; Saijo, K.; Takenaka, M.; Hashimoto, T. Ordering of Cylindrical Domains of Block Copolymers under Moving Temperature Gradient: Separation of ∇T-Induced Ordering from Surface-Induced Ordering. *Macromolecules* **2008**, *41*, 6787–6792.

56. Mita, K.; Tanaka, H.; Saijo, K.; Takenaka, M.; Hashimoto, T. Macroscopically Oriented Lamellar Microdomains Created by "Cold Zone-Heating" Method Involving OOT. *Polymer* **2008**, *49*, 5146–5157.
57. Yager, K. G.; Fredin, N. J.; Zhang, X.; Berry, B. C.; Karim, A.; Jones, R. L. Evolution of Block-Copolymer Order through a Moving Thermal Zone. *Soft Matter* **2010**, *6*, 92–99.
58. Nassyrov, D.; Muller, C.; Roige, A.; Burgues-Ceballos, I.; Oriol Osso, J.; Amabilino, D. B.; Garriga, M.; Isabel Alonso, M.; Goni, A. R.; Campoy-Quiles, M. Vapour Printing: Patterning of the Optical and Electrical Properties of Organic Semiconductors in One Simple Step. *J. Mater. Chem.* **2012**, *22*, 4519–4526.
59. Burgués-Ceballos, I.; Campoy-Quiles, M.; Francesch, L.; Lacharmoise, P. D. Fast Annealing and Patterning of Polymer Solar Cells by Means of Vapor Printing. *J. Polym. Sci., Part B: Polym. Phys.* **2012**, *50*, 1245–1252.
60. Olszowka, V.; Hund, M.; Kuntermann, V.; Scherdel, S.; Tsarkova, L.; Boker, A.; Krausch, G. Large Scale Alignment of a Lamellar Block Copolymer Thin Film *via* Electric Fields: A Time-Resolved SFM Study. *Soft Matter* **2006**, *2*, 1089–1094.
61. Konrad, M.; Knoll, A.; Krausch, G.; Magerle, R. Volume Imaging of an Ultrathin SBS Triblock Copolymer Film. *Macromolecules* **2000**, *33*, 5518–5523.
62. Brandrup, J.; Immergut, E. H.; Grulke, E. A.; Abe, A.; Bloch, D. R. *Polymer Handbook*, 4th ed.; John Wiley & Sons: New York, 1999.
63. Yokoyama, H.; Mates, T. E.; Kramer, E. J. Structure of Asymmetric Diblock Copolymers in Thin Films. *Macromolecules* **2000**, *33*, 1888–1898.
64. Khanna, V.; Cochran, E. W.; Hexemer, A.; Stein, G. E.; Fredrickson, G. H.; Kramer, E. J.; Li, X.; Wang, J.; Hahn, S. F. Effect of Chain Architecture and Surface Energies on the Ordering Behavior of Lamellar and Cylinder Forming Block Copolymers. *Macromolecules* **2006**, *39*, 9346–9356.
65. Matsen, M. W. Architectural Effect on the Surface Tension of an ABA Triblock Copolymer Melt. *Macromolecules* **2010**, *43*, 1671–1674.
66. Coulon, G.; Russell, T. P.; Deline, V. R.; Green, P. F. Surface-Induced Orientation of Symmetric, Diblock Copolymers: A Secondary Ion Mass-Spectrometry Study. *Macromolecules* **1989**, *22*, 2581–2589.
67. van Dijk, M. A.; van den Berg, R. Ordering Phenomena in Thin Block Copolymer Films Studied Using Atomic Force Microscopy. *Macromolecules* **1995**, *28*, 6773–6778.
68. Paik, M. Y.; Bosworth, J. K.; Smilges, D.-M.; Schwartz, E. L.; Andre, X.; Ober, C. K. Reversible Morphology Control in Block Copolymer Films *via* Solvent Vapor Processing: An *In Situ* GISAXS Study. *Macromolecules* **2010**, *43*, 4253–4260.
69. Stafford, C. M.; Roskov, K. E.; Epps, T. H., III; Fasolka, M. J. Generating Thickness Gradients of Thin Polymer Films *via* Flow Coating. *Rev. Sci. Instrum.* **2006**, *77*, 023908.
70. Fetters, L. J.; Lohse, D. J.; Richter, D.; Witten, T. A.; Zirkel, A. Connection between Polymer Molecular Weight, Density, Chain Dimensions, and Melt Viscoelastic Properties. *Macromolecules* **1994**, *27*, 4639–4647.